REPORT DOCUMENTATION PAGE

Form Approved
OMB NO. 0704-0188

1. AGENCY USE ONLY *(Leave Blank)*	2. REPORT DATE	3. REPORT TYPE AND DATES COVERED
	11 May 2001	Final 22 Sep 1997 – 21 Sep 2000

4. TITLE AND SUBTITLE
Simulation of Nonequilibrium Rocket Motor Plumes

5. FUNDING NUMBERS
DAAG55-97-1-0406

6. AUTHORS(S)
Graham V. Candler

7. PERFORMING ORGANIZATiION NAMES(S) AND ADDRESS(ES)
University of Minnesota
Aerospace Engineering and Mechanics
110 Union St. SE
Minneapolis, MN 55455

8. PERFORMING ORGANIZATION REPORT NUMBER

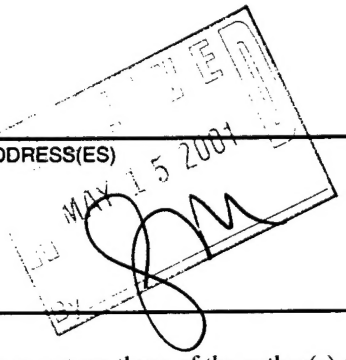

9. SPONSORING / MONITORING AGENCY NAME(S) AND ADDRESS(ES)
U.S. Army Research Office
P.O. Box 12211
Research Triangle Park, NC 27709-2211

10. SPONSORING / MONITORING AGENCY REPORT NUMBER
37556.3-EG-SDI

11. SUPPLEMENTARY NOTES
The views, opinions and/or findings contained in this report are those of the author(s) and should not be construed as an official Department of the Army position, policy or decision, unless so designated by other documentation.

12a. DISTRIBUTION / AVAILABILITY STATEMENT
Approved for public release; distribution unlimited.

12b. DISTRIBUTION CODE

13. ABSTRACT *(Maxiumum 200 words)*

The research used parallelized computational fluid dynamics methods to make high fidelity simulations of thermo-chemical nonequilibrium flows in rocket motor plumes. This work had two main topics: recent thermal radiative emission experimental data from an Atlas launch were analyzed using a thermo-chemical model with finite-rate internal energy relaxation and chemical reactions. In addition, a detailed analysis of high-temperature flow fields were performed using a vibrational and electronic state-specific excitation model. The simulation results were then used to compute the ultraviolet and infrared radiation emitted from the high-temperature flows to compare with the recent measurements.

20010607 037

14. SUBJECT TERMS	15. NUMBER OF PAGES 29
	16. PRICE CODE

17. SECURITY CLASSIFICATION OR REPORT	18. SECURITY CLASSIFICATION OF THIS PAGE	19. SECURITY CLASSIFICATION OF ABSTRACT	20. LIMITATION OF ABSTRACT
UNCLASSIFIED	UNCLASSIFIED	UNCLASSIFIED	UL

SIMULATION OF NONEQUILIBRIUM ROCKET PLUME FLOWS

FINAL REPORT

Graham V. Candler

May 11, 2001

U. S. ARMY RESEARCH OFFICE

Grant No. DAAG55-97-1-0406

University of Minnesota, Minneapolis MN 55455

Approved for Public Release;
Distribution Unlimited

STATEMENT OF THE PROBLEM STUDIED

The research used parallelized computational fluid dynamics methods to make high fidelity simulations of thermo-chemical nonequilibrium flows in rocket motor plumes. This work had two main topics: recent thermal radiative emission experimental data from an Atlas launch were analyzed using a thermo-chemical model with finite-rate internal energy relaxation and chemical reactions. In addition, a detailed analysis of high-temperature flow fields were performed using a vibrational and electronic state-specific excitation model. The simulation results were then used to compute the ultraviolet and infrared radiation emitted from the high-temperature flows to compare with the recent measurements.

SUMMARY OF MOST IMPORTANT RESULTS

This report summarizes the results of this study, with most focus on the analysis of the Atlas II motor plumes. Additional information may be found in the papers cited and in the recent Ph.D. thesis written by Dr. Krishnendu Sinha [1].

To summarize this work, the most important findings were:

1. The numerical simulation of rocket motor plumes remains a very challenging task. Even with advanced implicit parallel methods, the combined effects of chemical reactions, turbulence, and the vast range of length scales makes the simulations difficult.
2. The level of turbulent kinetic energy assumed to be in the exit plane of the motor exhaust is critical to predicting the level of radiative emission from the plume. This not so much an effect of turbulence itself, but is due to changing the total energy of the flow in the nozzle exit plane.
3. For the simulations performed, other than the effect just mentioned, the effect of turbulence on the flow was fairly minimal.
4. The numerical methods and gridding used for the plume simulations are critical. We found that third-order accurate methods were required to obtain sufficiently accurate results, even with multi-million point grids. The effects of the grid singularities on the nozzle grid axes is a major problem that has not been overcome with existing methods. Solving this problem remains a major challenge and should be the subject of a separate study.
5. The topology of the rocket motor plumes is very dependent on the altitude; this effect is reproduced by the simulations, and the change in the nature of the emission from the flow fields is also captured.

6. The low-altitude (15 km) simulations that we performed were extremely challenging due to very stringent grid requirements, very thin shear layers, and rapid chemical kinetics. The simulations resulted in plumes with a large-scale unsteadiness present. This effect is representative of the actual physical situation, though the calculations were not designed to capture unsteady effects. See the more detailed information below for further discussion.

7. The presence of soot in the motor exhaust is a critical element in the generation of the signature and the change in the signature from low to high altitude. A more detailed model of soot oxidation should be included in the simulations to allow the soot signal to be reduced downstream of the nozzle exit plane. This would increase the accuracy of the simulations performed to date.

8. The k-ϵ turbulence model equations are difficult to solve for these high Mach number flows with thin, high-intensity shear layers. We modified the conventional linearization of the source terms in the k-ϵ model; this resulted in at least a factor of ten reduction in the cost of these calculations.

9. The use of the overlay method for the simulation of complex chemically reacting flows is straight-forward and very powerful. Essentially arbitrarily complex chemical kinetics models can be solved to predict the emission from trace species in plumes and hypersonic vehicle flow fields.

The following report discusses these findings in more detail. Additional information may be found in the cited publications.

ATLAS II ROCKET MOTOR PLUME SIMULATIONS

Plume Geometries

The plume geometry is the same as that used in previous papers [1,2] The nozzle structure consists of a linear arrangement of three nozzles: a pair of booster nozzles surround the low pressure sustainer nozzle. All nozzles have a radius of 0.66 m, and are separated by 1.524 m (center-to center). Since all of the nozzles are co-linear, only one-fourth of the domain must be modeled due to symmetry. A cross-section of the computational domain for the Atlas-II plume is shown in Fig. 1. Care was taken to locate a grid line at the edges of the booster and sustainer nozzles in order to reduce the numerical error at the interface between the nozzle and free-stream flows. If the grid lines cross this interface, the plume is artificially diffused and deformed due to numerical error.

The computational grid has three grid blocks: in Fig. 1, the red grid has $54 \times 70 \times 294$ points, and represents the sustainer and part of the free-stream flow; the green grid has $82 \times 22 \times 294$ points and comprises the booster flow; the blue grid has $102 \times 82 \times 294$ points and represents the outer plume and free-stream flow. The latter grid is stretched away from the plume centerline so that the entire plume is contained within the grid. The grid is stretched in the axial direction away from the nozzle, with some clustering in the vicinity of the first shock reflection point at the centerline. This 4.1 million point grid represents a balance between accurately resolving the complex flow and the computational cost.

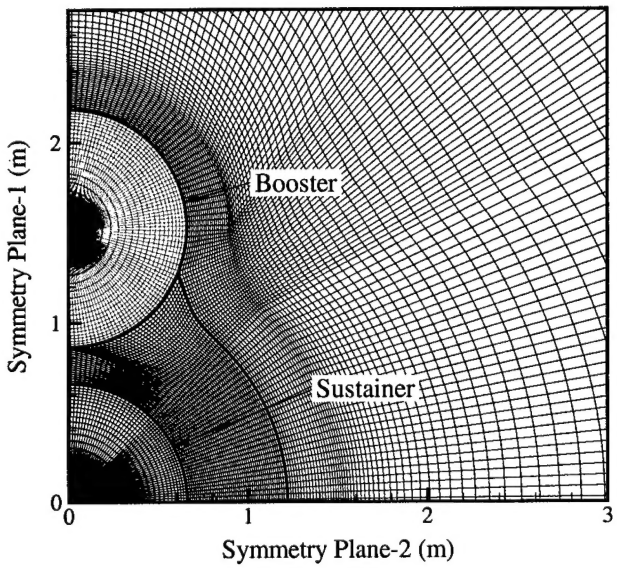

FIGURE 1. Cross-section of the computational grid at the nozzle exit plane.

A single axisymmetric-equivalent nozzle with the same mass and energy flow is used for studies of grid resolution, numerical methods, and turbulence modeling parameters.

Numerical Method

The plume flow fields are simulated by solving the three-dimensional Favre-averaged Navier-Stokes equations for reacting flows using the implicit full matrix Data-Parallel Lower-Upper Relaxation (DP-LUR) method [4]. Finite-rate chemistry effects are included using a nine-species model (CO_2, H_2O, CO, N_2, O_2, H_2, OH, O, H) with ten reactions [5].

The simulations are for Atlas-II flight conditions at two altitudes: 15 and 40 km. Free-stream, booster, and sustainer properties at the computed conditions are summarized in Table 1. The rotational modes are assumed to be in equilibrium with the translational modes. Vibrational nonequilibrium is allowed through the solution of a vibrational energy conservation equation. Vibrational relaxation rates are taken from Millikan and White [6] and are used in the standard Landau-Teller source term. The Park two-temperature vibration-dissociation coupling model is used [7]. Species viscosities and thermal conductivities are calculated via least squares curve fits to experimental data [8,9], and the mixture values are then determined using Wilke's mixing rule [10]. Diffusion coefficients are calculated using Fick's Law.

	15 km	40 km	Single Nozzle	Booster	Sustainer
Velocity (m/s)	535	1476	2960	2930	3280
Pressure (N/m^2)	12100	278	68850	78410	20200
Temperature (K)	217	251	2230	2380	1684
Mass Fractions:					
CO_2	0.000458	0.000458	0.302262	0.324814	0.337660
H_2O	0.000000	0.000000	0.272443	0.280699	0.249950
CO	0.000000	0.000000	0.412135	0.381744	0.396997
N_2	0.766388	0.766388	0.000000	0.000000	0.000000
O_2	0.233154	0.233154	0.000028	0.000175	0.000000
H_2	0.000000	0.000000	0.012194	0.009945	0.015381
OH	0.000000	0.000000	0.000797	0.002319	0.000007
O	0.000000	0.000000	0.000014	0.000067	0.000000
H	0.000000	0.000000	0.000127	0.000237	0.000005

TABLE 1. Free-stream and nozzle exit conditions at 15 and 40 km.

The numerical fluxes are evaluated using a third-order accurate MUSCL [11] modified Steger-Warming scheme [12]. Tests indicate that a second-order differencing scheme

becomes unstable near the axis degeneracies (located at the nozzle centerlines with the present grid topology). This is due to numerical error accumulation and amplification near the axis. We have tested several third-order accurate differencing schemes and found them to be more suitable and stable near the axis. Hence, a third-order scheme is used. The use of this high-order accurate differencing method significantly reduces the grid requirements.

In all of the cases presented in this paper the numerical simulation begins at the exit plane of the motor nozzles, and a simple supersonic inflow boundary condition is assumed. A hyperbolic tangent function is used to smooth flow gradients between the nozzle and free-stream. This type of smoothing was previously shown to be required to obtain a grid-independent solution [2].

Turbulence Modeling

The turbulent flow is simulated using the Favre-averaged Navier-Stokes equations along with the high Reynolds number version of the $k-\epsilon$ turbulence model of Jones and Launder [13]. The conservation equations for the turbulent kinetic energy, k, and solenoidal part of the turbulent dissipation, ϵ_s, are as follows.

$$\frac{\partial \bar{\rho} k}{\partial t} + \frac{\partial \bar{\rho} \tilde{u}_j k}{\partial x_j} - \frac{\partial}{\partial x_j}\left[\left(\mu + \frac{\mu_T}{\sigma_k}\right)\frac{\partial k}{\partial x_j}\right] = \mathcal{P}_k - \bar{\rho}\epsilon_s - \bar{\rho}\epsilon_c + \overline{p'' d''}$$

$$\frac{\partial \bar{\rho} \epsilon_s}{\partial t} + \frac{\partial \bar{\rho} \tilde{u}_j \epsilon_s}{\partial x_j} - \frac{\partial}{\partial x_j}\left[\left(\mu + \frac{\mu_T}{\sigma_\epsilon}\right)\frac{\partial \epsilon_s}{\partial x_j}\right] = c_1 \frac{\epsilon_s}{k}\mathcal{P}_k - c_2 \frac{\epsilon_s}{k}\bar{\rho}\epsilon_s$$

Here, $\bar{\rho}$ is the average density, $\tilde{u}_i$ represents the mass-averaged velocity and μ is the molecular viscosity. The turbulent viscosity, μ_T, is modeled as

$$\mu_T = c_\mu \frac{\rho k^2}{\epsilon_s + \epsilon_c}$$

where ϵ_c is the compressible dissipation. Following the Sarkar and Lakshmanan model [14],

$$\epsilon_c = \alpha_1 M_t^2 \epsilon_s$$

where $M_t^2 = 2k/\gamma RT$ is the turbulent Mach number. The production of turbulent kinetic energy, $\mathcal{P}_k$, is given in terms of the Reynolds stress tensor, τ_{ij},

$$\mathcal{P}_k = \tau_{ij}\frac{\partial \tilde{u}_i}{\partial x_j}$$

and the pressure-dilatation term, $\overline{p''d''}$, is modeled as [15]

$$\overline{p''d''} = -\alpha_2 M_t^2 \mathcal{P}_k + \alpha_3 M_t^2 \bar{\rho} \epsilon_s \ .$$

In order to improve predictions of axisymmetric jets, two modifications are suggested by Dash [16]. The first modifies the value of the model constant c_1, and the second introduces an extra term in the ϵ equation. Among the various forms presented in literature, the term proposed by Pope [17] is favored because of its basis in vortex stretching arguments. However, Lakshmanan and Abdol-Hamid [18] found that these extra terms deteriorate the model predictions for axisymmetric turbulent jets. Therefore, this extra term is not added to the ϵ-equation in the present study. The model constants used are

$$\begin{aligned} &c_\mu = 0.09, \quad c_1 = 1.60, \quad c_2 = 1.92, \\ &\sigma_k = 1.0, \quad \sigma_\epsilon = 1.3, \\ &\alpha_1 = 1.0, \quad \alpha_2 = 0.4, \quad \alpha_3 = 0.2. \end{aligned}$$

Axisymmetric Parametric Studies

Turbulent flow computations require the free-stream values of k and ϵ, which in this case correspond to the exit plane of the nozzle. Without any experimental data for the nozzle exit conditions, we need to choose reasonable values of the turbulent kinetic energy and dissipation. In order to assess the effect of the inflow k and ϵ on the solution, we performed a series of parametric studies using an axisymmetric plume geometry at conditions corresponding the 40 km altitude.

First, we fixed the value of k_∞ such that the turbulent intensity, $T_i = k/U^2$, is equal to 0.01, and then varied ϵ_∞ over a range of reasonable values. Figure 2 shows the contours of the computed turbulent kinetic energy. We see that the flow with $\epsilon_\infty = 18 \times 10^9 \ \mathrm{m}^2/\mathrm{s}^2$ (which corresponds to $\mu_T/\mu_\infty = 50$, where μ_∞ is the molecular viscosity at the plume exit plane) has very low levels of k. However, the other four turbulent simulations have significant levels of turbulent kinetic energy, with most k production occurring in the shear layer and downstream of the barrel shock reflection.

Comparing the five turbulent flows, we see that decreasing ϵ_∞ results in increased turbulent kinetic energy production, except for the case with the lowest level of inflow turbulent dissipation. Thus there is a threshold value of ϵ_∞ required to sustain the turbulence.

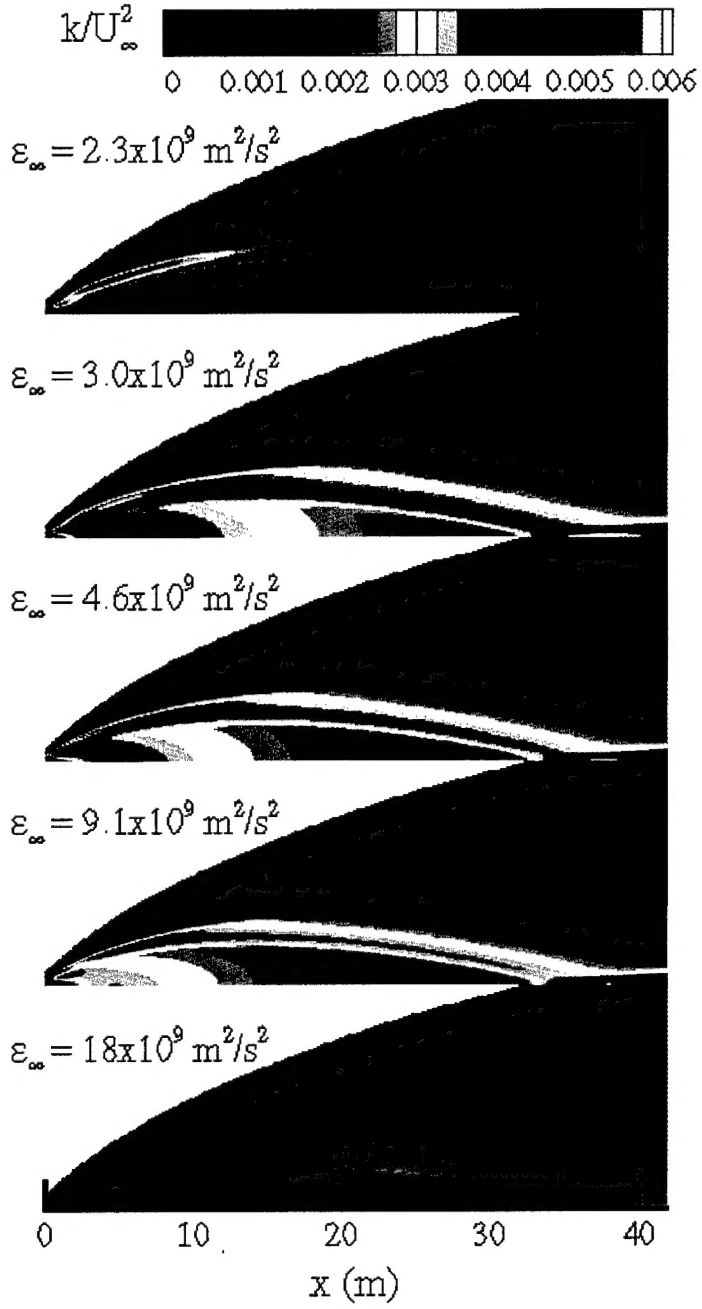

FIGURE 2. Normalized turbulent kinetic energy (k/U_∞^2) in the axisymmetric plume for different values of ϵ_∞ and $T_i = 1\%$.

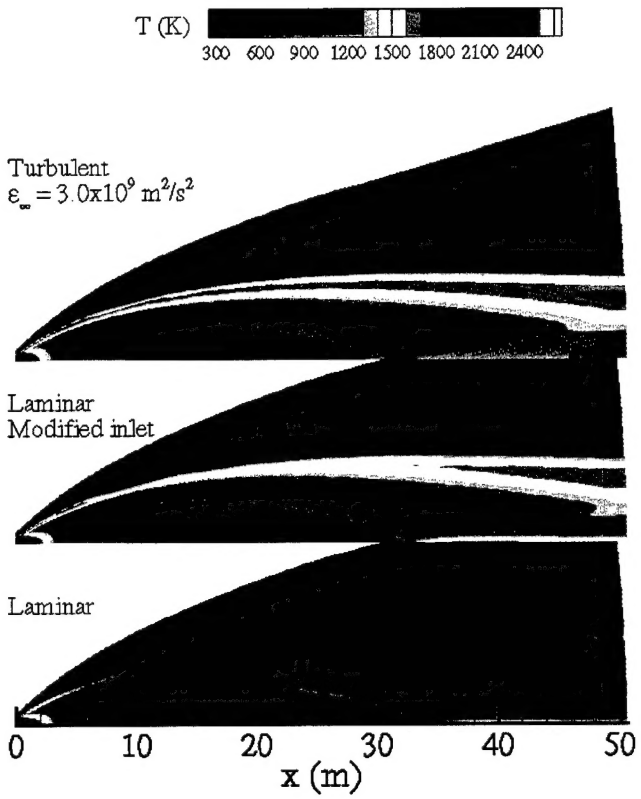

FIGURE 3. Temperature for the laminar flow, the laminar flow with modified plume inflow conditions, and a turbulent flow ($T_i = 1\%$, $\epsilon_\infty = 3.0 \times 10^9\ \mathrm{m}^2/\mathrm{s}^2$).

The temperature levels in the plume shear layer for all the turbulent cases increase by a few hundred degrees in comparison to the laminar plume, but there is very little variation between the turbulent cases themselves. The number density of OH follows the temperature trend, thus we see a higher OH concentration in the turbulent cases, but relatively little variation between the turbulent cases. From this study, we conclude that ϵ_∞ has an effect on the turbulence level in the plume, but the temperature and species concentrations are not significantly affected by ϵ_∞.

In the cases discussed above, the inflow turbulent energy is taken to be 1% of the average kinetic energy of the flow. Thus, the overall inflow energy in the turbulent simulations is higher than that in the laminar computation. If we study the turbulent flows in the region close to the inlet, we see that in all cases, the turbulent kinetic energy decays initially and this extra energy is distributed to the other energy modes. To assess the effect of this additional energy, we simulated a laminar case with the extra energy added to the nozzle exit plane conditions. Figure 3 compares computed temperature for the regular laminar

solution, the laminar flow with the additional inflow energy, and a turbulent flow with $\epsilon_\infty = 3.0 \times 10^9\,\mathrm{m}^2/\mathrm{s}^2$. We see that the increase in temperature in the modified laminar case is comparable to that in the turbulent case, showing that the extra energy introduced in the form of either k_∞ or modified nozzle exit conditions is the primary cause of the increased temperature and the resulting higher product concentration in the shear layer. Figure 4 plots the temperature and OH number density across the shear layer in these three flows. Even a small amount of extra energy over the nozzle exit conditions is enough to cause a few hundred degrees temperature variation in the shear layer. As a result, the OH number density changes by two orders of magnitude. Therefore, the primary effect of turbulence in this calculation is the added energy, rather than the increased dissipation in the shear layer.

Next, we study the effect of variation in k_∞ on the plume flow field. We find that there is a gradual increase in the peak temperature and a corresponding increase in the OH number density as we increase k_∞. However, this increase is small compared to that shown in Fig. 4, and thus increases in the turbulence intensity beyond 1% do not have a significant effect under these conditions. Finally, we study the effect of grid spacing on the $k - \epsilon$ turbulence model. We find that refining the grid increases the level of turbulence, but with a sufficiently fine grid, the solution is grid independent.

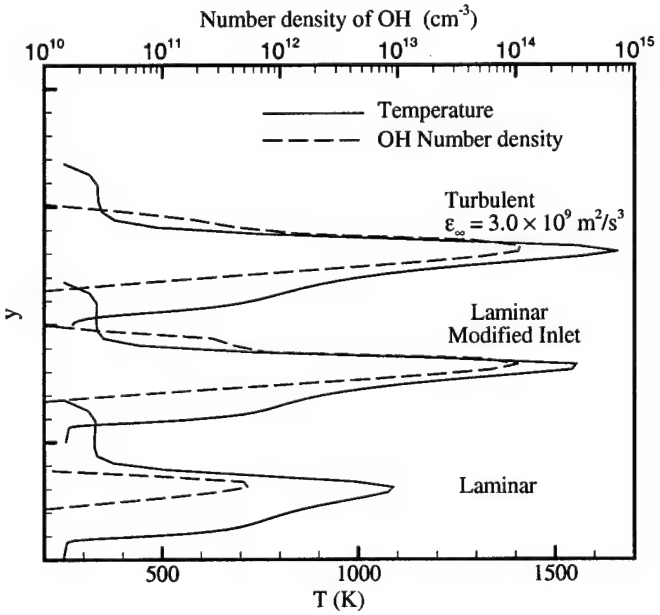

FIGURE 4. Temperature and OH number density across the shear layer in the regular laminar flow, the laminar flow with modified inlet conditions, and a turbulent turbulent flow ($T_i = 1\%$, $\epsilon_\infty = 3.0 \times 10^9\,\mathrm{m}^2/\mathrm{s}^2$).

Three-Dimensional Atlas-II Plumes

In this section we discuss the results of numerical simulations of three-dimensional Atlas-II plumes at two flight conditions: 15 and 40 km altitude. The 40 km results were reported in a previous paper [3], but it is interesting to contrast these results with the lower altitude results. Both flight conditions have been computed with a laminar flow model and the two-equation turbulence model discussed above.

The results presented here are primarily in the form of temperature and OH number density contours. This gives a qualitative description of the flow fields and shows how the different flight conditions affect the overall flow topology. The results have been used to compute the radiative emission from the Atlas-II flow fields to compare with emission measurements [19].

The turbulent cases were initialized by the turbulence quantities that gave the highest turbulence intensities in the shear layer for the axisymmetric 40 km plume ($T_i = 1\%$ and $\epsilon_\infty = 3.0 \times 10^9\,\mathrm{m}^2/\mathrm{s}^2$).

It is not possible to perform a rigorous grid resolution study for this problem because the current 4.1 million point grid is already expensive to use. This grid was constructed based on the results of the grid convergence studies performed in the previous papers [2,3], but with the additional benefit of using a third-order accurate upwind-biased method, rather than a pure upwind second-order method. Thus, the present results should be sufficiently well resolved.

15 km Altitude Flight Condition Results

Figure 5 plots contours of the temperature and the logarithm of the OH number density in the two symmetry planes; parts (a) and (b) show the results in the plane of the nozzle centerlines; (c) and (d) in the plane perpendicular to the nozzle axis plane.

Figure 5(a) shows that at the 15 km conditions, the turbulence modeling does not affect the spreading of the plume appreciably. The high temperature regions in the plume are confined to the shear layer between the plume and the external flow, until about 70 m from the nozzle exit; at that point the high temperature region expands to almost the entire plume core. This spreading of the high-temperature region appears to be related to the formation of unstable vortical structures downstream of the 50 m point. It would appear that this instability should not be permitted by the implicit time integration method. However, we have performed parametric studies to understand how the formation of the unstable vortical structures is affected by the time step used in the calculation. We find

that there is no discernible difference between the largest numerically stable time step and significantly smaller integration steps. This is not surprising because the time step is governed by the regions of the flow with much finer mesh spacing than in the region of the instabilities. Thus, the time integration is very accurate in this region.

It is completely reasonable that the plume shear layers become unstable and form large-scale structures, as seen in the calculations. However, these calculations were not designed for the simulation of shear layer instability growth. This would require at a minimum a full 360° flow field simulation to capture wave growth, a careful initialization of the inflow to include fluctuations at appropriate modes, and a low dissipation numerical method. Thus the present results are of questionable validity. On the other hand, the results point to the fact that the flow is unsteady, and needs to be simulated using an advanced method such as a large-eddy simulation (LES) or a detached eddy simulation (DES).

The OH number density plot shows an apparently more diffuse plume, however this is largely a result of plotting the logarithm of n_{OH}. The substantial concentrations of OH are confined to the plume core, and largely occur in regions of elevated temperature. The presence of the unstable vortical structures is also apparent in this plot.

The plume structure is substantially different in the second symmetry plane, as seen in Figs. 5(a) and (b). The high-temperature region is more tightly confined to the plume centerline, but the plume has a larger spreading rate from the axis. This is also reflected in the OH concentration, but again plotting the logarithm enhances the apparent plume spreading rate. The more rapid spreading is a result of the two high-pressure booster motor flows compressing the lower pressure sustainer motor flow; the resulting high pressure gas expands off-axis and causes enhanced plume growth in this plane.

The unstable nature of the plume is again apparent in this plot, but the shear layer appears to be unstable closer to the nozzle exit plane, at about 30 m. The large-scale high-temperature off-axis regions downstream of about 70 m are formed by the unstable vortical structures; these high-temperature regions propagate downstream at about the local axial flow speed.

These results are reflected in the temperatures and OH number densities plotted in cross-sections of the plume, as seen in Fig. 6. For simplicity, only the turbulent flow results are plotted here. Close to the nozzle exit plane (Fig. 6(a) at 4.6 m), the primary flow structure are the shear layers at the edge of the booster motor flows. The sustainer motor flow is strongly compressed near the plume centerline at this point, which is upstream of

the primary shock reflection point. Small-scale kinks in the shear layer can be seen near the interaction between the booster and sustainer motor flows; their cause is unknown. Further from the nozzle exit plane, the flow has taken on a very complicated structure with a wide range of scales, as seen in Fig. 6(b) (located 56 m from the nozzle axis). Very complicated shear layers have been formed as the shocks reflect from the plume centerline, the primary shear layer, and other flow structures. Further downstream (Fig. 6(c)), the plume has spread significantly and the range of scales of the structures has been reduced due to mixing and diffusion. As seen in the streamwise contour plots (Fig. 5), the plume spreads more in the transverse plane, although the higher temperature regions are more aligned with the nozzle axis plane.

40 km Altitude Flight Condition Results

Figure 7 plots the same quantities as Fig. 5, but at conditions corresponding to 40 km altitude. Here the external flow speed is higher, but more importantly, the difference between the nozzle exit pressure and the free-stream is much greater. This results in a more diffuse shear layer and a barrel shock reflection point much farther downstream. The plume is entirely steady for both the laminar and turbulent calculations, and the primary difference between the two calculations is probably due to the additional inflow energy that is represented by the 1% turbulence intensity. Again, we see that the plume spreads more rapidly in the off-nozzle-axis direction; in this case this effect is amplified.

Figure 8 plots the temperature and OH concentration in the cross-sectional plane located at 160 m from the nozzle exit plane. We see that the plume structure is quite different at the higher altitude. This figure clarifies that the plume spreads much more extensively in the plane perpendicular to the nozzle axis. There is one large nearly circular high temperature shear layer centered at the plume axis, and two smaller nearly circular lobes expanding in the transverse plane. Interestingly, the peak temperature and OH concentration occur in the secondary lobes.

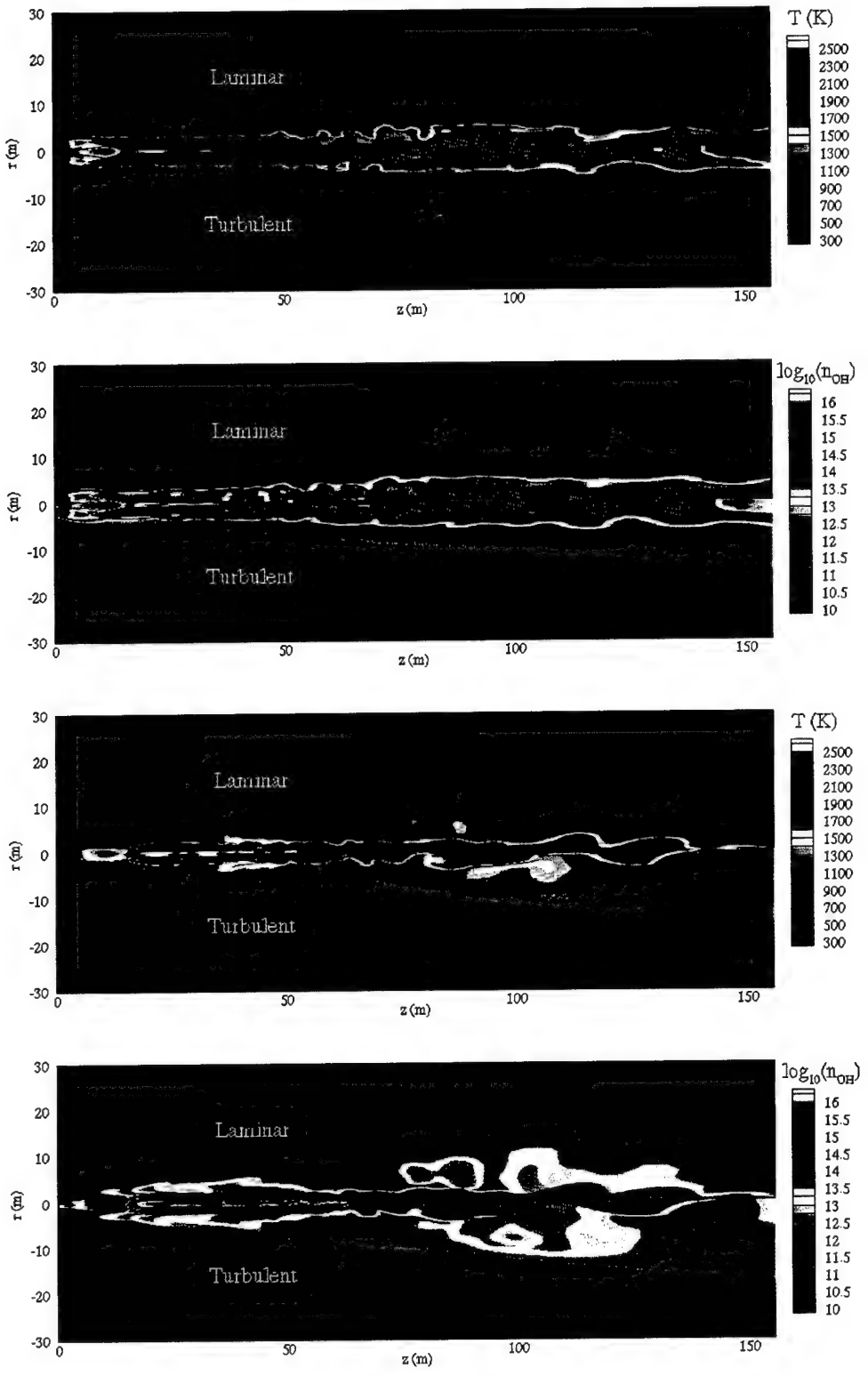

FIGURE 5. 15 km altitude results: (a) temperature and (b) OH concentration in nozzle axis plane; (c) temperature and (d) OH concentration in transverse symmetry plane. Top: laminar solution; bottom: $k - \epsilon$ solution.

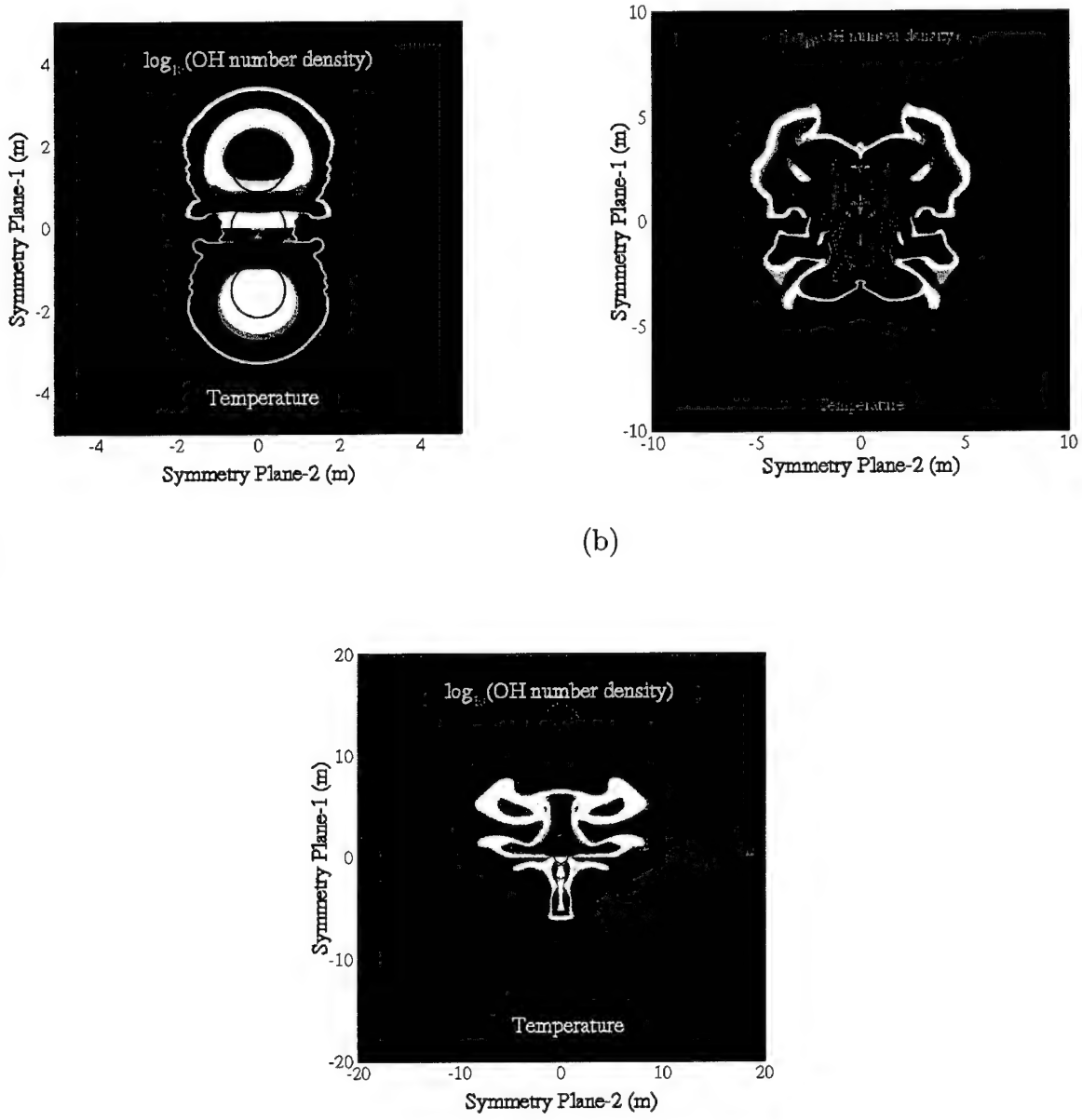

(a) (b)

(c)

FIGURE 6. Temperature and OH number density contours in three cross-sectional planes of the Atlas-II plume at 15 km: (a) 4.6 m; (b) 56 m; and (c) 160 m from the nozzle exit plane.

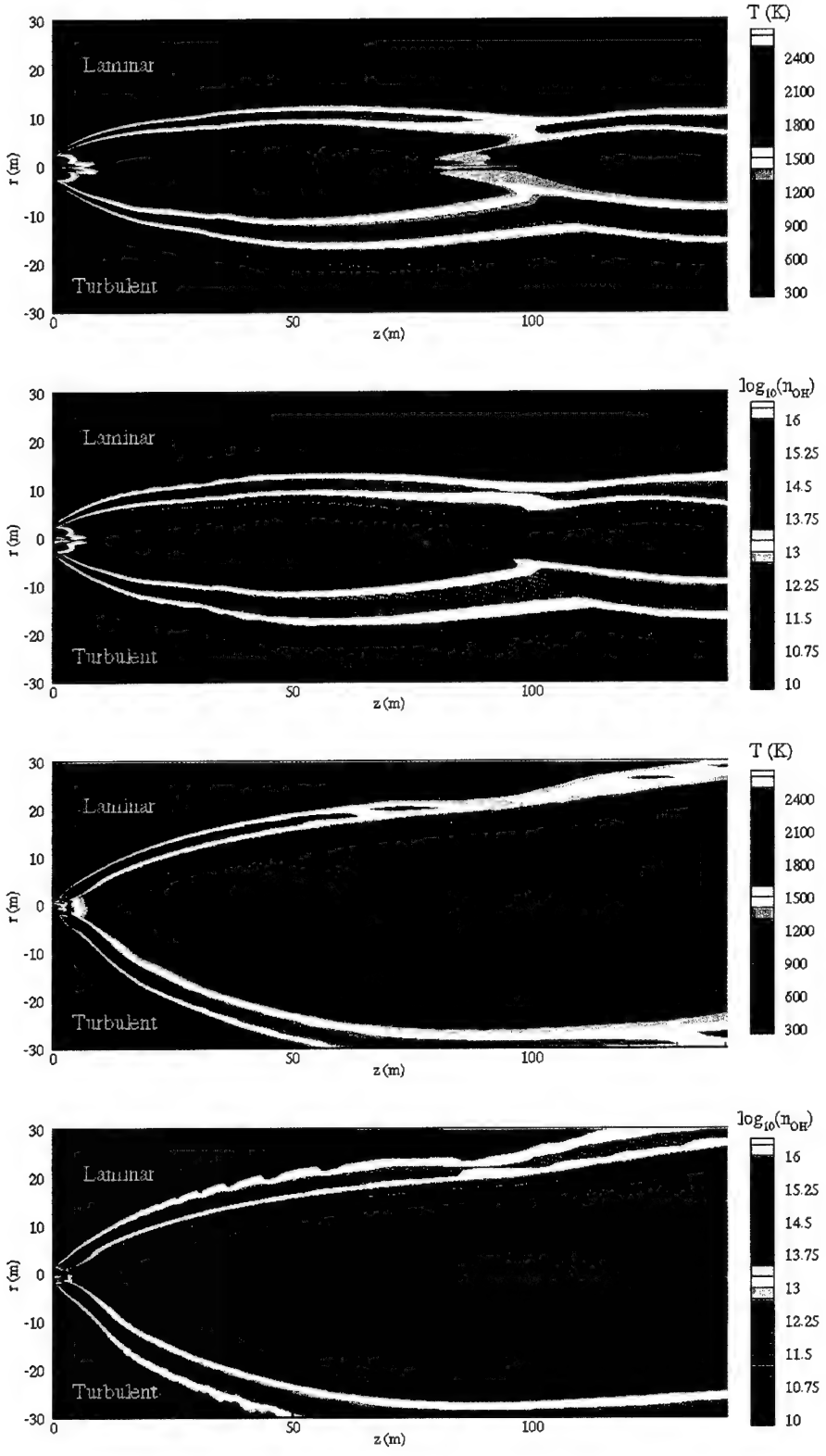

FIGURE 7. 40 km altitude results: (a) temperature and (b) OH concentration in nozzle axis plane; (c) temperature and (d) OH concentration in transverse symmetry plane. Top: laminar solution; bottom: $k - \epsilon$ solution.

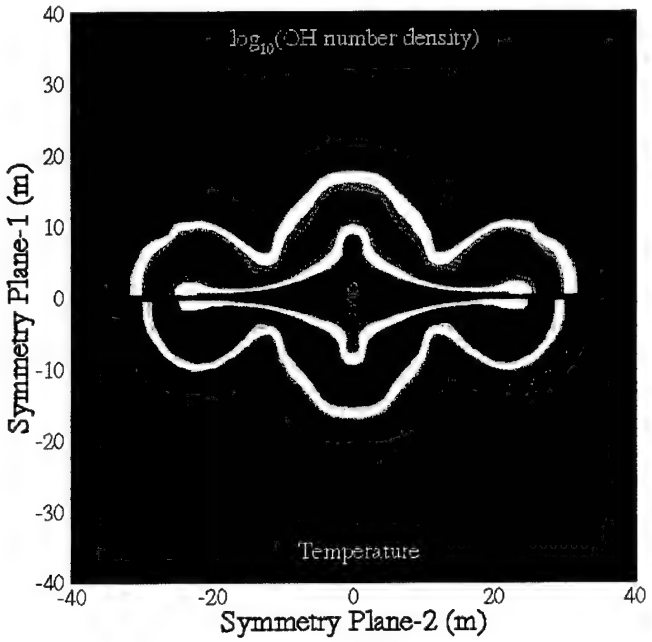

FIGURE 8. Temperature and OH number density contours in a cross-sectional plane 160 m from the nozzle exit plane of the Atlas-II plume at 40 km.

Summary

Numerical simulations of Atlas-II plumes have been performed at two flight conditions using a third-order accurate upwind-biased method with implicit time integration. A nine-species finite-rate chemical reaction model was used. These are flying plume simulations, in that the effects of the hardbody are not included. Care was taken to align the grid with the nozzle lip to significantly reduce the numerical spreading of the plume. This required the use of a 4.1 million point grid composed of three different grid blocks. Even with an efficiently parallelized code, a significant amount of computer time was required to obtain these solutions. The 15 km altitude case is particularly demanding because of the thin shear layers, large turbulence model source terms, and rapid chemical reactions at these conditions.

Both laminar and two-equation turbulence model simulations were performed. The major difference between these different transport models appears to be the result of adding turbulent kinetic energy to the plume inflow for the turbulent simulations. The plumes tend to spread more quickly in the plane perpendicular to the nozzle axis plane; this is particularly true for the 40 km case, where two high-temperature off-axis lobes are formed. The primary shear layers in the 15 km altitude case become unstable in our calculations,

resulting in the formation of large-scale structures that convect downstream through the plume core. These structures are regions of high temperature and OH concentration, which will significantly affect the plume signature. However, the numerical simulations were designed to capture these unsteady effects, and an appropriate numerical approach should be used for more accurate predictions of their behavior.

The results of these simulations were used to predict the emission from the plumes at 15 and 40 km altitudes. These results were presented in [20] and a paper has been prepared and submitted for publication [21].

OVERLAY APPROACH FOR STATE-SPECIFIC SIMULATIONS

As part of the research project, an overlay method was developed and tested for the simulation of flows with trace chemical species. The flow about a hypersonic vehicle or a rocket motor plume can be modeled in two steps. First, the flow field is simulated by solving the Navier-Stokes equations that have been extended to include the effects of finite-rate chemical reactions and internal energy relaxation. This solution includes all of the chemical species that may be present in large amounts, or those that are important in the chemical kinetics of those major species. Then, the mass conservation equations for the trace chemical species are overlaid on the previously-computed flow field. Since the trace species are present in very small amounts, they do not affect the mass, momentum, or energy of the bulk flow.

The computational fluid dynamics method that was used to simulate the flow of the major species in the stagnation region of a re-entry experiment and in the plume of the thrusting rocket has been discussed above. For example, consider a baseline model for air that is a reacting mixture of thermally perfect gases composed of the following chemical species: N_2, O_2, NO, N, and O. These species are allowed to react with one another at finite rates. Here NO is included as a major species because it may be present in relatively large amounts and because is acts as a reaction intermediary in the Zeldovich reactions. The internal energy is described by translational, rotational, and vibrational temperatures. Finite-rate relaxation of the rotational and vibrational temperatures to the translational temperature is also modeled.

The flow is assumed to be described by the extended Navier-Stokes equations, which for two-dimensional flows may be written in conservation law form as

$$\frac{\partial U}{\partial t} + \frac{\partial F}{\partial x} + \frac{\partial G}{\partial y} = W, \tag{1}$$

where U is the vector of conserved quantities, F and G are the flux vectors in the x and y directions, respectively, and W is the source vector due to chemical reactions and the relaxation of the vibrational and rotational temperatures toward the translational temperature. More details concerning the form of the fluxes and the source vector may be found in [22]. The numerical method for the solution of Eq. (1) uses modified Steger-Warming flux vector splitting, and the steady-state solution is obtained using implicit Gauss-Seidel line-relaxation [12]. The method has been validated by comparison to a wide range of experimental data. The flow properties thus obtained will be hereafter referred to as the "bulk solution."

If the argument is made that the introduction of trace species into the bulk flow does

not affect the energy or momentum of the bulk solution, then a simplified conservation law for these "overlay" species can be written,

$$\frac{\partial \rho_s}{\partial t} + \frac{\partial}{\partial x}(\rho_s u + \rho_s \hat{u}_s) + \frac{\partial}{\partial y}(\rho_s v + \rho_s \hat{v}_s) = w_s, \qquad s = 1, 2, \ldots, n_s \tag{2}$$

where s is the index of each of the n_s overlay species, ρ_s is the species mass density, w_s is the chemical source term, u and v are the mass-averaged flow velocities in the x and y directions, and $\hat{u}_s$ and $\hat{v}_s$ are the diffusion velocities of species s. The mass-averaged velocities are obtained from the bulk solution, as are the densities of the major species and the temperatures that appear in the chemical source term. Hence, once the steady-state bulk solution has been obtained, Eq. (2) can be solved. Note that the overlay approach could also be used to add additional internal energy conservation equations, provided that the energy contained in these modes is small compared to the total energy.

To make this decomposition of the flow field into a bulk solution and an overlay solution, we have assumed that the overlay species do not alter the state of the bulk solution appreciably. There are three criteria that must be met for this condition to hold. First, the trace species must be present in small amounts so that only a small fraction of the mass is missing from the bulk flow solution. Secondly, the presence of the trace species cannot affect the diffusion coefficients of the bulk species. A very light overlay species, such as H, could possibly alter the mass diffusion coefficient of the heavy bulk species if it was present in large mass fractions. However, as the overlay species are present in only trace amounts, this is not an important effect. Thirdly, and most importantly, the overlay species cannot affect the chemical kinetics of the bulk species. For example, NO may be present in only small amounts, but it may be the most efficient reaction path for the dissociation of N_2. Therefore, it cannot be treated as an overlay species unless N_2 dissociation is not important under the conditions of the simulation. In practice, with the appropriate choice of the overlay species, we can apply this method when the trace species are present at levels of less than about 10^{-4} mass fraction, which would produce errors of less than 0.1% in the bulk solution properties.

The solution of Eq. (2) is much less costly than the solution of Eq. (1) would be if both the bulk and overlay species were included. This is because the cost of solving Eqs. (1) and (2) scale approximately as the square of the number of equations being solved. By solving two smaller sets of equations the computational cost is reduced. Also, aside from the source terms, Eq. (2) is linear in ρ_s making it easier to solve. Also note that the flux-vector splitting is dramatically simplified because the flux Jacobian is a diagonal matrix, and therefore the evaluation of the fluxes is trivial. Also, many of the components of the

source terms can be computed once and stored for use in all subsequent time steps during convergence to steady-state. Therefore, the cost per iteration of the overlay equations is considerably less than that of the full equation set. In practice, the overlay equation set usually converges to a steady-state with about a factor of ten fewer iterations than the bulk solution. Thus, it is possible to incorporate detailed excited state chemistry models in the overlay solution.

To illustrate the power of the overlay approach, the results we summarize the results of a paper published under the support of this grant [23]. In this work, the overlay method was used to model the vibrational state distributions of NO, CO, water, and CO_2, which are potential shock-layer radiators in the midwave IR. The spectral predictions show that radiation from shock heated ambient CO_2 will be an important contribution at most altitudes and speeds slower than 3.5 km/s. This work included a detailed vibrational state-specific model of CO_2 excitation. Comparisons of the spatial distributions of CO_2 vibrational states with a corresponding Boltzmann distribution at the translational temperature show that there are substantial differences in the populations. These predictions are important for the design of an upcoming sounding rocket experiment.

IMPROVEMENTS TO TWO-EQUATION TURBULENCE MODELING FOR COMPRESSIBLE FLOWS

In order to simulate a compressible turbulent flow using the $k-\epsilon$ turbulence model, we need to solve the Reynolds-averaged equations governing the mean flow along with the transport equations for the turbulent kinetic energy, k, and the dissipation rate, ϵ. To account for the turbulence-chemistry interactions, we may need to solve an additional transport equation for the energy variance.

The standard k-ϵ model, developed for high Reynolds number flows, was originally used along with wall functions to account for the viscous effects near a solid boundary. On the other hand, the low Reynolds number versions of the model allow integration of the equations through the viscous near-wall region, thus enabling computation of complex flows in which wall functions are not valid. However, a very fine grid is needed near the wall to resolve the strong gradients of k and ϵ in this region, and therefore the computation becomes expensive. In addition, these strong gradients make the non-linear low Reynolds number terms numerically very stiff. As a result, the time-step is limited to small values and the solution requires a large number of iterations to converge. This increases the computational cost even further. As a result, the simulation of turbulent flows using k-ϵ models becomes very computationally intensive.

There are a wide variety of numerical methods used to simulate turbulent flows using the k-ϵ turbulence model. The methods can be broadly categorized into two groups: explicit methods and implicit methods. The explicit methods are simple but the time-step is limited to very small values. As a result, the solution requires an extremely large number of iterations to reach the steady-state. On the other hand, the implicit methods circumvent the time-step restriction by linearizing the equations. Larger time-steps can, therefore, be taken and the solution converges in fewer iterations. The convergence rate depends on an accurate linearization of the equations. Therefore, the convergence properties of a method may be degraded when the low Reynolds number, Re, terms are not linearized. Moreover, these terms are noted to be numerically stiff. Therefore, not linearizing them is expected to deteriorate convergence significantly.

Implicit Formulation

For an explicit formulation the time-step is severely restricted by the CFL condition ($\Delta t < \Delta x/(|\hat{u}| + a)$). An implicit method circumvents this restriction by evaluating the fluxes and source terms at the future time-level t^{n+1} instead of t^n. The fluxes and the source terms at t^{n+1} are obtained by linearization; this process is well documented in the

literature.

Here we consider the source terms, which are given by P_k, $\mathcal{L}_k$ and $\mathcal{L}_\epsilon$. The expressions for these terms are quite extensive and linearizing all the terms is a cumbersome task. Moreover, in case of an external flow with a turbulent boundary layer, only the body-normal derivatives, $\partial/\partial\eta$, are important. This fact is used to identify the dominant contributions to the source terms.

$$P_k \simeq \mu_T \left(\frac{\partial \tilde{u}}{\partial \eta}\right)^2, \quad \mathcal{L}_k \simeq 2\bar{\mu} \left(\frac{\partial \sqrt{k}}{\partial \eta}\right)^2, \quad \mathcal{L}_\epsilon \simeq \frac{2\bar{\mu}\mu_T}{\bar{\rho}} \left(\frac{\partial^2 \tilde{u}}{\partial \eta^2}\right)^2.$$

We use a Mach 2.244 boundary layer as a test case. Fig. 9 presents the convergence history of the solution for the four different conventional implicit methods. The convergence properties of Vandromme's method is very similar to our method which implies that linearizing μ_T does not affect the convergence much. The variation of μ_T is important for the production of turbulence, and hence proper linearization of μ_T is expected to be essential for better convergence. However, linearizing μ_T in P_k results in a negative diagonal contribution to the Jacobian matrix and is destabilizing. The reason for little effect of linearizing μ_T on the convergence may be because of these two effects counteracting each other.

Comparison of the convergence histories of the decoupled method and the current method shows that decoupling the turbulent source terms from the mean flow does not affect the convergence rate significantly. This means that the variation in the source terms is mainly determined by the development of the turbulence variables k and ϵ. However, in case of the method that does not linearize $\mathcal{L}_k$ and $\mathcal{L}_\epsilon$, convergence is much slower than the other three methods. This implies that the low Re terms are numerically very stiff and need to be linearized in order to achieve good convergence rates.

In the computation of the Mach 2.244 boundary layer using the conventional methods which linearize $\mathcal{L}_k$ and $\mathcal{L}_\epsilon$, the solution requires about 4000 iterations to converge. The computational time, although not prohibitive, is quite large for a simple flow computation with relatively small number of points (100×100 grid). Increasing the number of points in the i-direction to 200 and 400 requires 16,000 and 50,000 iterations, respectively. Thus, the computational time become substantial in these cases. Therefore, the convergence properties of these conventional methods are far from satisfactory. In order to identify the problem that causes poor convergence, we studied the development of the solution in terms of the variation of the residual. In Fig. 9, the initial drop in the residual corresponds to the development of a laminar boundary layer on the plate. The velocity gradients in the

laminar boundary layer trigger the turbulent production mechanisms and large quantities of turbulent kinetic energy are produced. This corresponds to the rise in the value of the residual around iteration 600. Once sufficient turbulence has developed, the residual starts decreasing again (around iteration 1300). Although the decay of the residual is fairly steady, the residual frequently increases in the form of sharp peaks. We will refer to these peaks as "spikes" in the residual history. The time-step is limited by these spikes and therefore, the solution requires a large number of iterations to converge. In addition, the time-step needs to be continuously monitored and frequently reduced (Table 6.1) so that the spikes do not become large and cause the solution to diverge. These spikes are present in case of all the methods used and they result in slower convergence. Thus, the key to improve the convergence rates is to eliminate the spikes.

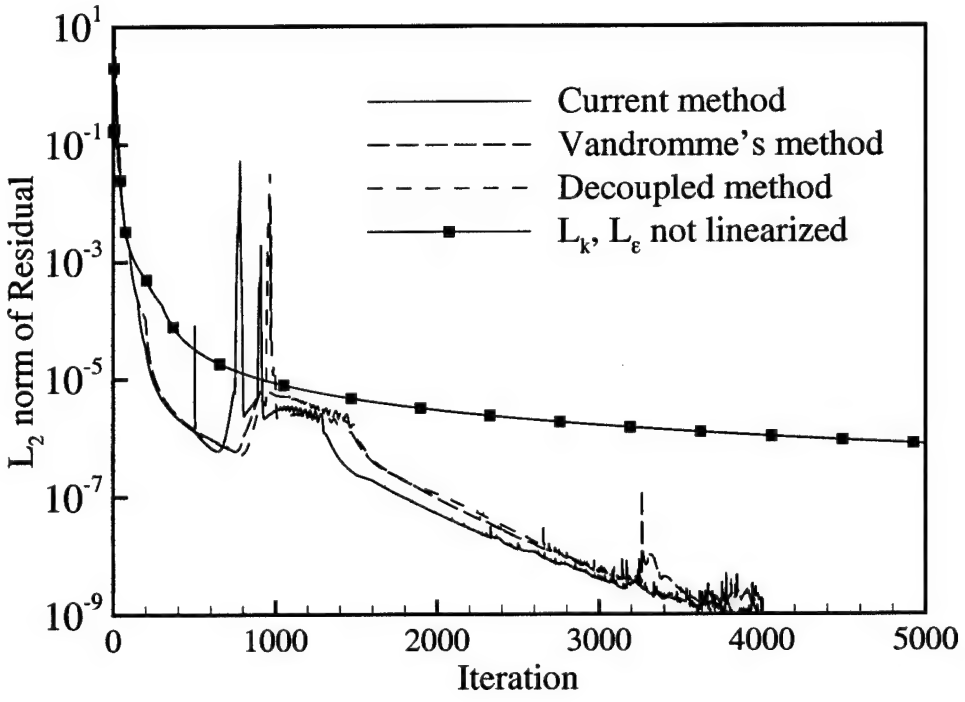

FIGURE 9. Comparison of convergence characteristics of several conventional methods in case of a Mach 2.244 turbulent boundary layer computation.

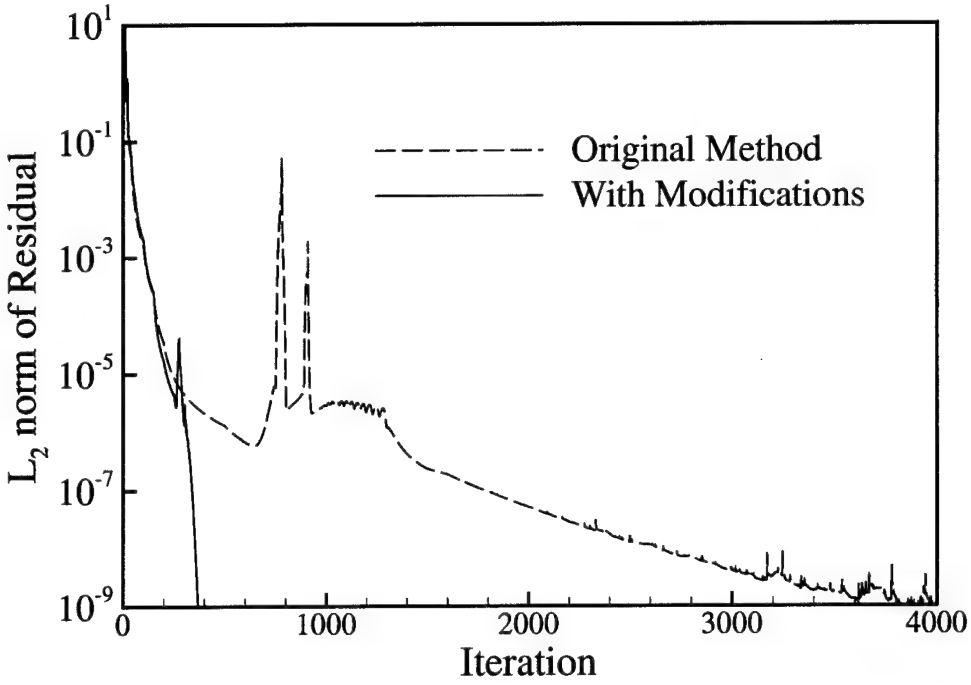

FIGURE 10. Convergence history of the Mach 2.244 boundary layer solution computed using the original method (the box represents the magnified view shown in Fig. 13).

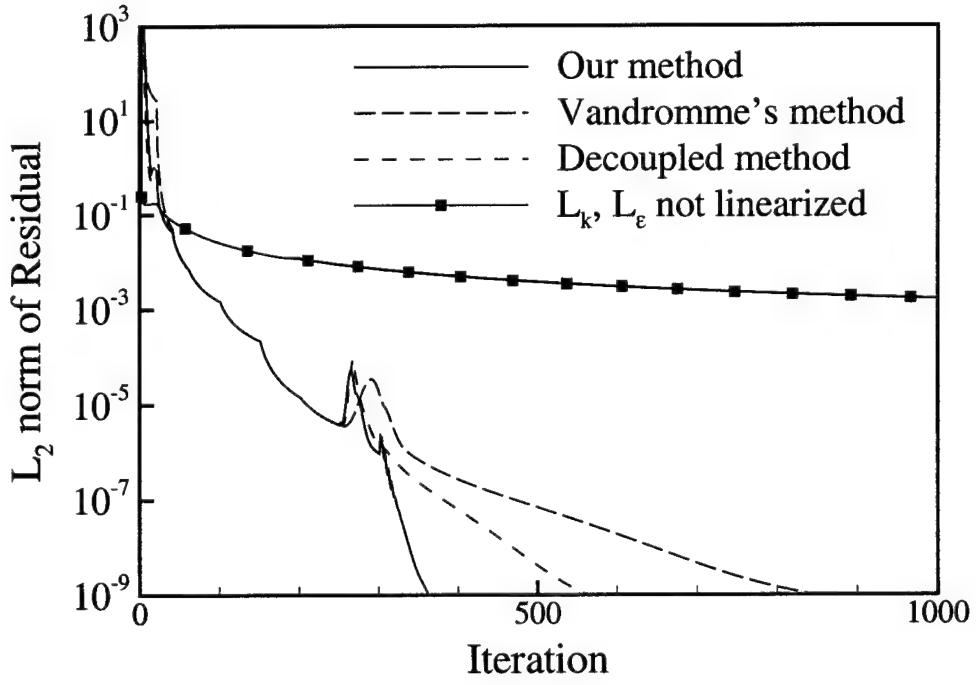

FIGURE 11. Effect of the modifications on the convergence characteristics of conventional methods in the computation of the Mach 2.244 boundary layer.

We stabilized the spikes in two ways: the central difference in the Jacobian of $\mathcal{L}_k$ is replaced by stable one-sided differences, and a low value of turbulent dissipation is used in the free-stream. The Mach 2.244 boundary layer is computed using this modified method and the convergence history is compared with that of the original method in Fig. 10. We can see that the spikes in the residual history are eliminated and the only rise in the residual corresponds to the initial buildup of turbulence. The final time-step can be increased by two orders of magnitude, and the steady-state solution is reached in less than 400 iterations. Thus, the computational time is reduced by a factor of 10. Applying the modifications to Vandromme's method and the decoupled method shows similar improvements (Fig. 11). In these cases, the number of iterations is reduced by factors of 5 and 8, respectively. However, the method which does not linearize $\mathcal{L}_k$ and $\mathcal{L}_\epsilon$ does not show any improvement. This is because of the fact that the modifications in the Jacobian of $\mathcal{L}_k$ does not affect this numerical method.

These modifications, and in particular, the change in the differencing method for $\mathcal{L}_k$, to the implicit formulation result in dramatic reductions in the computational time required to obtain solutions of complex flows. Moreover, the time step does not have to be continually adjusted to control the formation of the spikes, resulting in a much less monitoring of the calculation. This too results in a large reduction in the difficulty of performing these calculations. This approach was used in the k-ϵ simulations of the plumes discussed previously in this report. Without this approach, those calculations would have been dramatically more difficult to obtain. Further information about the modifications to the implicit method can be found in [1].

REFERENCES

[1] Sinha, K., *Analysis of the k-epsilon Turbulence Model for Simulation of Compressible Flows,* Ph.D. Thesis, Department of Aerospace Engineering and Mechanics, University of Minnesota, March 2001.

[2] Wright, M.J., Rao, R.M., Candler, G.V., Hong, J.S., Schilling, T.A., Levin, D.A., "Modeling Issues in the Computation of Plume Radiation Signatures," AIAA Paper No. 98-3622, July 1998.

[3] Rao, R.M, Sinha, K., Candler, G.V., Wright, M.J., and Levin, D.A., "Numerical Simulations of Atlas II Rocket Motor Plumes," AIAA Paper No. 99-2258, June 1999.

[4] Wright, M.J., Candler, G.V., and Prampolini, M., "Data-Parallel Lower-Upper Relaxation Method for the Navier-Stokes Equations," *AIAA J.,* Vol. 34, No. 7, 1996, pp. 1371-1377.

[5] Hong, J.S., Levin, D.A., Collins, R.J., Emery, J., and Tietjen, A., "Comparison of Atlas Ground Based Plume Imagery with Chemically Reacting Flow Solutions," AIAA Paper No. 97-2537, June 1997.

[6] Millikan, R.C. and White, D.R., "Systematics of Vibrational Relaxation," *J. Chem. Phys,* Vol. 39, Oct. 1963, pp. 3209-3213.

[7] Park, C., "Assessment of Two-Temperature Kinetic Model for Dissociating and Weakly Ionizing Nitrogen," AIAA Paper No. 86-1347, June 1986.

[8] Svehla, R.A., "Estimated Viscosities and Thermal Conductivities of Gases at High Temperatures," NASA TR R-132, 1962.

[9] McBride, B.J., Gordon, S., and Reno, M.A., "Coefficients for Calculating Thermodynamic and Transport Properties of Individual Species," NASA TM 4513, Oct. 1993.

[10] Wilke, C.R., "A Viscosity Equation for Gas Mixtures," *J. Chem. Phys,* Vol. 18, No. 4, 1950, pp. 517-519.

[11] Yee, H.C., "A Class of High-Resolution Explicit and Implicit Shock Capturing Methods," NASA TM 101088, 1989.

[12] MacCormack, R.W. and Candler, G.V., "The Solution of the Navier-Stokes Equations Using Gauss-Seidel Line Relaxation," *Computers and Fluids,* Vol. 17, No. 1, Jan. 1989, pp. 135-150.

[13] Jones, W.P., and Launder, B.E., "The Prediction of Laminarization with a Two-Equation model of Turbulence," *Int. J. Heat Mass Transfer,* Vol. 15, 1972, pp. 301-

314.

[14] Sarkar, S., and Lakshmanan, B., "Application of a Reynolds Stress Turbulence Model to the Compressible Shear Layer", *AIAA J.*, May 1991, pp. 743-749.

[15] Sarkar, S., "Modeling the Pressure-Dilatation Correlation", NASA CR 187566, May 1991.

[16] Dash, S.M., "Observations on Practical Turbulence Modeling for High-Speed Jet / Plume Flowfields", AIAA Paper No. 91-1789, June 1991.

[17] Pope, S.B., "An Explanation of the Turbulent Round-Jet/Plane-Jet Anomaly", *AIAA J.*, Mar 1978, pp. 279-281.

[18] Lakshmanan, B., and Abdol-Hamid, K.S.,"Investi- gation of Supersonic Jet Plumes using an Improved Two-Equation Turbulence Model", *J. Prop. Power*, Vol. 10, No. 5, Sep. 1994, pp. 736-741.

[19] Alexeenko, A., Collins, R.J., Gimelshein, S., Levin, D.A., Hong, J.S., and Schilling, T.A., "Modeling of Radiation in the Atlas Plume-Flow," AIAA Paper No. 2001-0355, Jan. 2001.

[20] Alexeenko, A.A., N.E. Gimelshein, D.A. Levin, R.J. Collins, R. Rao, G.V. Candler, J.S. Hong, and T. Schilling, "Modeling of Radiation in Atlas Plume Flow," *AIAA Paper No. 2001-0355,* Jan. 2001.

[21] Alexeenko, A.A., N.E. Gimelshein, D.A. Levin, R.J. Collins, R. Rao, G.V. Candler, J.S. Hong, and T. Schilling, "Modeling of Flow and Radiation in the Atlas Plume," submitted for publication in the *Journal of Thermophysics and Heat Transfer,* April 2001.

[22] Candler, G.V. and R.W. MacCormack, "The Computation of Hypersonic Ionized Flows in Chemical and Thermal Nonequilibrium," *Journal of Thermophysics and Heat Transfer,* Vol. 5, No. 3, pp. 266-273, July 1991.

[23] Levin, D., G.V. Candler, and C. Limbaugh, "Multispectral Shock-Layer Radiance from a Hypersonic Slender Body," *Journal of Thermophysics and Heat Transfer,* Vol. 14, No. 2, pp. 237-243, Apr.-June 2000. Also *AIAA Paper No. 99-3747,* Jan. 1999.

LIST OF PUBLICATIONS

1. Sinha, K., and G.V. Candler, "An Accurate Implicit Formulation of a Two-Equation Turbulence Model," *AIAA Paper No. 98-2649,* June 1998.

2. Wright, M.J., G.V. Candler, J. Hong, and D.A. Levin, "An Efficient Parallel Method for Rocket Plume Simulations," *AIAA Paper No. 98-3622,* July 1998.

3. Rao, R.M., K. Sinha, G.V. Candler, M.J. Wright, D.A. Levin, and J.Hong, "Numerical Simulations of Atlas II Rocket Plumes," *AIAA Paper No. 99-2258,* June 1999.

4. Levin, D., G.V. Candler, and C. Limbaugh, "Multispectral Shock-Layer Radiance from a Hypersonic Slender Body," *Journal of Thermophysics and Heat Transfer,* Vol. 14, No. 2, pp. 237-243, Apr.-June 2000. Also *AIAA Paper No. 99-3747,* Jan. 1999.

5. Sinha, K., P. Martin, and G.V. Candler, "Assessment of Temperature Fluctuation Models for RANS Simulations of Hypersonic Reacting Flows," *AIAA Paper No. 2000-0537,* Jan. 2000.

6. Candler, G.V., R.M. Rao, K. Sinha, D.A. Levin, "Numerical Simulations of Atlas-II Rocket Motor Plumes," *AIAA Paper No. 2001-0354,* Jan. 2001.

7. Sinha, K., M.P. Martin, and G.V. Candler, "Assessment of Turbulence Models for Compressible Flows Using Direct Numerical Simulation Data," *AIAA Paper No. 2001-0730,* Jan. 2001.

8. Alexeenko, A.A., N.E. Gimelshein, D.A. Levin, R.J. Collins, R. Rao, G.V. Candler, J.S. Hong, and T. Schilling, "Modeling of Flow and Radiation in the Atlas Plume," submitted for publication in the *Journal of Thermophysics and Heat Transfer,* April 2001.

9. Sinha, K., *Analysis of the k-epsilon Turbulence Model for Simulation of Compressible Flows,* Ph.D. Thesis, Department of Aerospace Engineering and Mechanics, University of Minnesota, March 2001.

10. Sinha, K., P. Martin, G.V. Candler, and I. Marusic, "Assessment of Models for Reynolds Stress using Direct Simulation Data," *AIAA Paper No. 2001-2837,* June 2001.

PERSONNEL SUPPORTED

1. Graham V. Candler, Principal Investigator.

2. Ram Rao, Post-Doctoral Research Associate, University of Minnesota.

3. Krishnendu Sinha, Master's of Science in Aerospace Engineering and Ph. D. in Aerospace Engineering, University of Minnesota.
4. V. Gregory Weirs, Ph. D. in Aerospace Engineering, University of Minnesota.
5. Michael J. Wright, Post-Doctoral Research Associate, University of Minnesota.

REPORT OF INVENTIONS

None.